

# A Subdivision Transformation Method for Weakly Singular Boundary Integrals in Thin-structural Problem

Junjian HOU\*, Li ZENG\*, Yudong ZHONG\*, Dengfeng ZHAO\*, Mingyuan ZHAO\*\*

\*Henan Provincial Key Laboratory of Intelligent Manufacturing of Mechanical Equipment, Mechanical and Electrical Engineering Institute, Zhengzhou University of Light Industry, Zhengzhou, 450002, Henan, China,

E-mail: zhongyd@zzuli.edu.cn

\*\*Zhengzhou Senpeng Electronic Technology Co., LTD, Zhengzhou, 450052, Henan, China

<https://doi.org/10.5755/j02.mech.31683>

## 1. Introduction

Thin structures have very good bearing performance, high strength and stiffness, small weight and can bear a considerable load with a small thickness, which are widely used in engineering structures [1-3]. Such as components for automobile and ship structures that improve load-bearing capacity and reduce weight, coating structures that improve heat and wear resistance of metal surfaces, as a buffer and energy absorption component used in aerospace, rail transportation fields, etc. To ensure the force and material strength of thin structure, it is necessary to carry out numerical analysis of mechanical properties according to its geometric parameters.

The boundary element method (BEM) is a more accurate and effective method developed after finite element method. Different from the basic idea of the finite element method (FEM), BEM only divides the elements on the boundary of the domain and approximate the boundary conditions with the functions satisfying the governing equation [4-7]. Therefore, compared with the FEM [8, 9], BEM has the advantages of dimensionality reduction, fewer elements and simpler data preparation, which is suitable for solving stress concentration, infinite domain and semi-infinite domain problems [10, 11]. However, as the singularities of the kernel function in the boundary integral equation (BIE), the computational accuracy of weak singular integral directly affects the final results, so additional processing schemes must be given to remove these singularities to ensure the successful solution of BEM. Especially for thin-structural problems, poorly shaped elements (such as elements with large angles or narrow lengths) will appear in the discrete geometric model of thin structure [12-14], which will seriously affect the accuracy of singular and near singular integrals. Many works have been demonstrated that the near singular integrals can be accurately evaluated by analytical and semi-analytical methods [15, 16], Sinh and other nonlinear transformation methods [4, 17-19], etc. Therefore, accurate and effective calculation of weakly singular integral in BIE is the key to the implementation of boundary element analysis [20-23].

At present, there are many methods have been developed to handle the weak singular integrals, such as integral simplification method [24], element subdivision methods [25-26] and polar coordinate transformation methods [20, 27-31]. When the position of the source point is close to the boundaries of the element, the computational accuracy cannot be guaranteed only by using the coordinate

transformation method [32]. To obtain high calculation accuracy, the integral element needs to be subdivided into several integral blocks with good shape. And there are many element subdivision methods, such as the singular points directly connected to the element vertexes [12], interval block method [12], tree structure methods [25], etc. When these subdivision methods are employed, some integral blocks with poor shape (such as the integral blocks with large angle and large aspect ratio) will be subdivided, which increases the difficulty in dealing with singular integral and decrease the computational accuracy. In addition, the polar coordinate transformation is the key to removing the weak singularities of the integral of the kernel. It converts the surface integral into the double integral of circumferential and radial direction, and then transforms the integral of radial direction to eliminate the singularities. Therefore, when this transformational method is employed, it needs to recalculate the integral interval of the integral block in the radial and circumferential directions every time, which is more troublesome to implement [32].

In this paper, the weakly singular boundary integrals of the displacement kernel function in the BIE of elastic thin-structural problems are considered. When the BIE is discrete by several elements, for the numerical integration of a discrete element, firstly, the subdivision techniques of the quadrilateral elements are developed according to the location of the source point, the element shape and the nearest distance from the source point to the element; and then, based on this subdivision technology, a simpler coordinate transformation method is constructed to remove the weak singularities of the singular integral blocks obtained by the proposed subdivision technology. Compared with the conventional polar coordinate transformation method, the presented method does not need to calculate their integral interval and is simpler and more effective. Finally, the subdivision technology and coordinate transformation method are applied to the BEM analysis for the elastic structure to realize an accurate and effective solution to the thin-structural problems.

The outlines of the paper are as follows: the BIE and its numerical discretization of the thin-structural problems are described in section 2. In section 3, the treatment of the weakly singular integrals is presented in detail. The verification results of numerical examples are given in Section 4. At last, the conclusions are given.

## 2. The boundary integral equations for thin-structural problems

The BIE of 3D elastic analysis for thin-structural problems is shown in Eq. (1) [33].  $P$  and  $Q$  are the source and field points;  $c_{ij}(P)$  is a constant associated with the boundary type;  $u_{ij}^*(P, Q)$  and  $t_{ij}^*(P, Q)$  are the kernel function of displacement and traction, respectively, and their expressions are shown in Eq. (2) [34]:

$$c_{ij}(P)u_j(P) = \int_{\Gamma} u_{ij}^*(P, Q)t_j(Q)d\Gamma(Q) - \int_{\Gamma} t_{ij}^*(P, Q)u_j(Q)d\Gamma(Q), \quad (1)$$

$$u_{ij}^*(P, Q) = \frac{1}{16\pi G(1-\nu)r} [(3-4\nu)\delta_{ij} + r_i r_j], \quad (2)$$

$$t_{ij}^*(P, Q) = -\frac{1}{8\pi(1-\nu)r^2} \left\{ \begin{array}{l} \left[ \frac{\partial r}{\partial n} (1-2\nu)\delta_{ij} + r_i r_j \right] \\ -(1-2\nu)(r_i n_j - r_j n_i) \end{array} \right\},$$

where:  $G$  and  $\nu$  denote the shear modulus and Poisson's ratio;  $r$  is the distance from the source point to field point;  $u_j(Q)$  and  $t_j(Q)$  represent the variables of displacement and traction on the boundary  $\Gamma$ ;  $n_i$  and  $n_j$  are the components of the external normal vector in  $i$  and  $j$  direction, respectively. By discretizing the integral equation Eq. (1) with  $N$  elements, Eq. (1) can be expressed as:

$$c_{ij}(P)u_j(P) = \sum_{e=1}^N \left\{ \sum_{\alpha=1}^n t_j^\alpha \int_{\Gamma_e} u_{ij}^*(P, Q)N_\alpha(Q)d\Gamma(Q) \right\} - \sum_{e=1}^N \left\{ \sum_{\alpha=1}^n u_j^\alpha \int_{\Gamma_e} t_{ij}^*(P, Q)N_\alpha(Q)d\Gamma(Q) \right\}, \quad (3)$$

in which,  $n$  is the number of nodes on each element, and  $N_\alpha(Q)$  is the shape function of the  $\alpha$ th node on the element. It can be seen from Eq. (2), the integrals of the displacement kernel function have weak singularities, while the integrals of the traction kernel function have strong singularities. The numerical results have shown that strongly singular integrals can be accurately calculated by the approximate expansion method and regularization method [35, 36]. In this paper, the weakly singular integrals of the displacement kernel function are mainly considered.

## 3. The processing method of weak singular boundary integral

To construct the weak singularity elimination technique proposed in this paper, one discrete element  $\Gamma_e$  is considered at first, and the integral of the displacement kernel function is simplified into the following form (Eq. (4)). Where  $f(P, Q)$  is a smooth function without singularity;  $\phi(Q)$  is the corresponding shape function:

$$I(P) = \int_{\Gamma_e} \frac{f(P, Q)}{r} \phi(Q)d\Gamma_e. \quad (4)$$

We can see in Eq. (4), the weak singularity will arise when  $r$  is equal to zero. Additional schemes for handling weak singular integrals need to be considered. To

achieve the purpose of solving the weakly singular integral accurately, the element subdivision technique associated with the weak singular boundary integral needs to be considered at first.

### 3.1. The element subdivision technique for solving singular integrals

As the uncertainty of the position of the source point (which may fall on the interior, edges and vertices of the element), the subdivision method will be different. When the position of the source point is given, the nearest distance  $d$  from the source point to the edges of the element can be calculated. And then a very small quadrilateral with a length of  $0.2d$  is constructed near the source point and the source point is included in it.

In which, the selection of  $0.2d$  is an empirical value obtained from a numerical test to avoid mutual interference between integral blocks. The specific operations are as follows: Firstly, to ensure that the shape of the singular integral block is good, we need to choose a regular quadrilateral that includes the source points. The choice of side length of the quadrilateral is very important. Too large selection of the side length will lead to a too large singular integral region, which requires too many Gaussian points and reduces the computational efficiency. In addition, the interference between integral blocks should be avoided. Therefore, this paper starts from  $0.5d$ . In the selection, it is found that if the side length of the constructed quadrilateral is large, especially for the element whose source point  $S$  falls near the center, small integral blocks will be divided near the edge, and the density of integral blocks cannot be guaranteed, which is the reason why  $0.2d$  is selected as the side length of the small quadrilateral in this paper.

By extending the four sides of the small quadrilateral and intersecting the integral element, several quadrilateral integral blocks can be obtained. Take the quadrilateral element as an example, the specific subdivision schemes are shown in Figs. 1 - 5. Fig. 1 is the result of the first step subdivision when the source point falls on the vertex of the integral element.

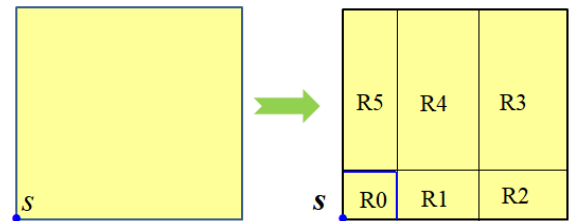


Fig. 1 The source point is located at the vertex

Fig. 2 shows the results of the first step subdivision when the source point falls on different locations of the edge, where Fig. 2, a is the result when the source point is near the vertex, Fig. 2, b is the near the vertex when the source point is away from the vertex. Fig. 3 shows several different cases of the first step subdivision when the source point falls inside the integral element. Figs. 3, a - c are the results when the source point is close to the vertex, the edge and the center, respectively.

In the second step, the vertices of the small quadrilateral containing the source point are connected with the source point, and several triangular integral blocks containing singular points  $S$  can be obtained (as show in Fig. 4). For

the sake of integral, the quadrilateral R1-R8 without source point in Figs. 1 - 3 should also be further subdivided. The subdivision method is as follows Fig. 5): If the value of  $l/d$  is less than 1, the integral block can be seen as a regular integral element. If  $l/d$  is greater than 1, the integral block is equally divided into four sub-elements. Repeat for sub-elements until all sub-elements are regular integral elements. Then the normal Gauss integral can be applied to the above regular integral elements.

In addition, if the shape of the integral element is narrow, the element can be subdivided according to the proportion of the longest ( $L_{max}$ ) and shortest edge ( $L_{min}$ ) of the element (as shown in Fig. 6, if  $L_{max}/L_{min} < 2$ , the element cannot be subdivided (Fig. 6, a). If  $2 < L_{max}/L_{min} < 3$ , the element needs to be divided into two integral sub-elements

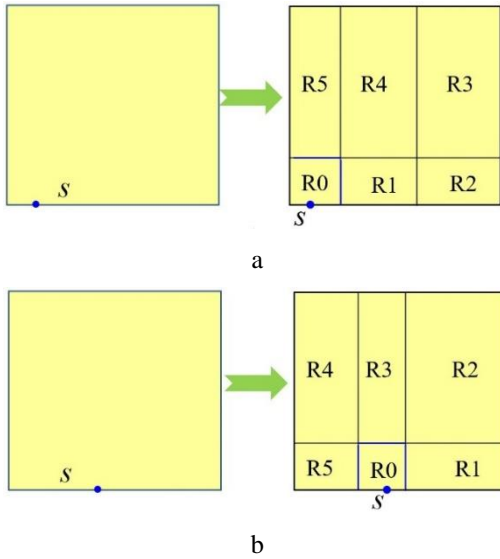


Fig. 2 The source point is located at the edge of the element

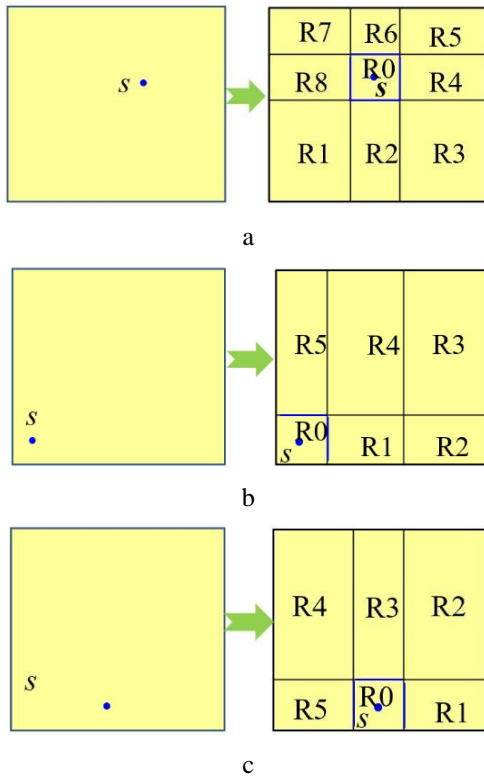


Fig. 3 The source point falls inside the element

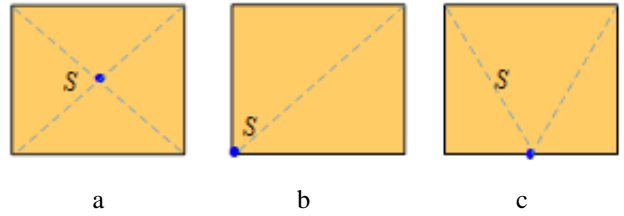


Fig. 4 The subdivision method of the small quadrilateral R0 containing source points

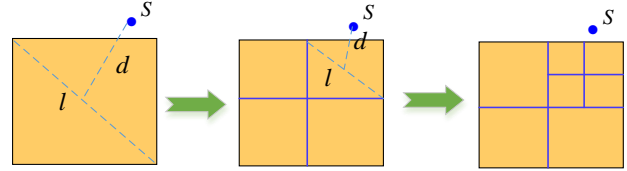


Fig. 5 The subdivision method of the quadrilateral R1-R8 without source point

(Fig. 6, b), and so on). And then the integral sub-elements with source points can be further subdivided according to the subdivision method in Figs. 1 - 3. Furthermore, if there is a slender integral block in the subdivision result (such as the slender quadrilateral integral block in Figs. 1 - 3), the integral block can still be further subdivided according to the method in Fig. 6, to ensure that there is no integral block with large aspect ratio in the subdivision results.

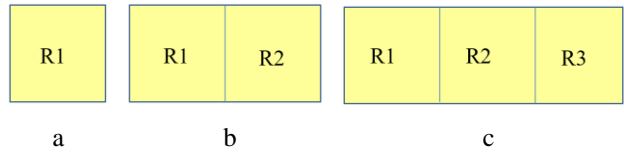


Fig. 6 The element subdivision method of slender quadrilateral elements

### 3.2 The elimination method of weak singularity

We can see from the above element subdivision method, the source points are first contained in a small quadrilateral, and then the vertices of the small quadrilateral are connected to the singular points, and four singular integral blocks are obtained at last.

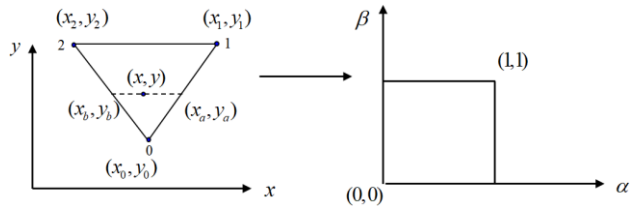


Fig. 7 The method of coordinate transformation of triangular integral blocks

The integral block without source points can be solved by conventional Gaussian integral. However, due to the singularity of the triangular integral block containing the source point, a simple Hammer integral cannot eliminate the singularity in the integrand, so it needs special treatment.

Taking Eq. (4) as the integral form, to remove the weak singularities of the integral block containing the source point, the  $(\alpha, \beta)$  local coordinate system is employed at first [37], and the corresponding mapping system is shown in Fig. 7. The specific process of the coordinate transformation method is as follows:

$$\begin{cases} x_a = x_0 + (x_1 - x_0)\alpha \\ y_a = y_0 + (y_1 - y_0)\alpha \end{cases} \quad (5)$$

$$\begin{cases} x_b = x_0 + (x_2 - x_0)\alpha \\ y_b = y_0 + (y_2 - y_0)\alpha \end{cases} \quad (6)$$

$$\begin{cases} x = x_a + (x_b - x_a)\beta \\ y = y_a + (y_b - y_a)\beta \end{cases} \quad \alpha, \beta \in [0,1]. \quad (7)$$

Substituting Eq. (5) and Eq. (6) into Eq. (7), the expression Eq. (8) can be derived:

$$\begin{cases} x = x_0 + (x_1 - x_0)\alpha + (x_2 - x_1)\alpha\beta \\ y = y_0 + (y_1 - y_0)\alpha + (y_2 - y_1)\alpha\beta \end{cases} \quad (8)$$

Through this transformation in Eq. (8), the integral block in the  $xy$  place is mapped into a regular quadrilateral in the  $\alpha\beta$  place. The coordinates of the two vertexes of the quadrilateral are (0,0) and (1,1), that is, the value range of the  $\alpha$  and  $\beta$  is [0,1]. The Jacobian of the transformation is  $\alpha S$ .

$$S = |x_0y_1 + x_1y_2 + x_2y_0 - x_0y_2 - x_1y_0 - x_2y_1|. \quad (9)$$

Through this transformation, the integral form of Eq. (4) in the triangular integral block with the singular points can be rewritten as:

$$\begin{aligned} I(Q) &= \int_{\Delta} \frac{f(P,Q)}{r} \phi(Q) d\Gamma = \\ &= \int_0^1 \int_0^1 \frac{Sf_2(\alpha, \beta)}{\sqrt{g(\alpha, \beta)}} \phi(Q) d\alpha d\beta, \end{aligned} \quad (10)$$

$$\begin{aligned} g(\alpha, \beta) &= ((x_1 - x_0)\alpha + (x_2 - x_1)\alpha\beta)^2 + \\ &+ ((y_1 - y_0)\alpha + (y_2 - y_1)\alpha\beta)^2. \end{aligned} \quad (11)$$

From Eqs. (5) - (9), we can see the Jacobian obtained by this coordinate transformation method contains quasi-zero factor  $\alpha$ , which just offsets the quasi-zero factor in the denominator of integral equation Eq. (4), and the singularity can be eliminated. Moreover, this coordinate transformation method can transform the integral interval of  $\alpha$  and  $\beta$  to [0,1] directly, which does not need to calculate the integral interval of each integral block. Compared with the traditional polar coordinate transformation, it is simpler and more effective.

#### 4. Numerical examples

In this part, three numerical examples are given to verify the accuracy and effectiveness of the proposed method. Firstly, the accuracy of the proposed method on one element is verified, where different source positions and element shape types are considered. Finally, the present method is employed to analyse the elastic analysis of the thin-structural problem. The computational formula of relative error is shown in Eq. (12):

$$\text{Relative Error} = \left| \frac{I_n - I_e}{I_e} \right|, \quad (12)$$

in which,  $I_n$  represents the numerical results and  $I_e$  is the corresponding reference solution. The reference solution is obtained by using the element subdivision coupled with the coordinate transformation method with a large number of Gaussian integral points. For the convenience of calculation, the paper assumes  $f(P,Q)=1.0$  in Eq. (4). The integral form Eq. (4) is applied to solve the weakly singular integrals in the first example.

##### 4.1. The integral element with different source points and aspect ratios

To verify the accuracy of the proposed method, the quadrilateral element with different source points and aspect ratios is considered. The four vertices of the quadrilateral element are (0.0, 0.0, 0.0), (1.0, 0.0, 0.0), (1.0, 1.0, 0.0) and (0.0, 1.0, 0.0), and the aspect ratio is  $a = 1$ .

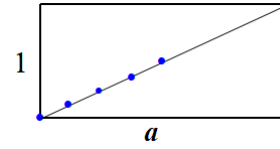


Fig. 8 The selections of the source points (aspect ratio is  $a$ )

Fig. 8 shows the selections of the source points, and the coordinates of the source points are taken as (0.0, 0.0, 0.0), (0.125, 0.125, 0.0), (0.25, 0.25, 0.0), (0.375, 0.375, 0.0) and (0.5, 0.5, 0.0), respectively. The relative errors and the total number of Gaussian points obtained by the proposed method and the traditional method (coordinate transformation coupled with the traditional element subdivision method, which the source point is directly connected with the vertexes of the element) are shown in Table 1.

Table 1

The results of singular integrals of quadrilateral elements ( $a=1$ )

Source points	Gaussian points	Proposed method	Gaussian points	Traditional method
(0.0,0.0,0.0)	128	5.44E-12	128	5.44E-12
(0.125,0.125,0.0)	448	6.35E-08	484	3.49E-05
(0.25,0.25,0.0)	448	1.07E-07	484	7.68E-07
(0.375,0.375,0.0)	448	1.48E-07	484	4.56E-09
(0.5,0.5,0.0)	256	2.51E-07	256	2.51E-07

When  $a = 2$ , the four vertexes of the quadrilateral element are given as (0.0, 0.0, 0.0), (2.0, 0.0, 0.0), (2.0, 1.0, 0.0) and (0.0, 1.0, 0.0). The source points are (0.0, 0.0), (0.25, 0.125, 0.0), (0.5, 0.25, 0.0), (0.75, 0.375, 0.0) and (1.0, 0.5, 0.0), respectively. The relative errors and the total number of Gaussian points of the weak singular integrals are as shown in Table 2.

When  $a = 5$ , the four vertexes of the quadrilateral element are given as (0.0, 0.0, 0.0), (5.0, 0.0, 0.0), (5.0, 1.0, 0.0) and (0.0, 1.0, 0.0). The source points are (0.0, 0.0), (0.625, 0.125, 0.0), (1.25, 0.25, 0.0), (1.875, 0.375, 0.0) and (2.5, 0.5, 0.0), respectively. The results of relative errors and the number of Gaussian integral points are shown in Table 3.

When  $a = 10$ , the four vertices of the quadrilateral element are given as  $(0.0, 0.0, 0.0)$ ,  $(10.0, 0.0, 0.0)$ ,  $(10.0, 1.0, 0.0)$  and  $(0.0, 1.0, 0.0)$ , the source points fall on  $(0.0, 0.0, 0.0)$ ,  $(1.25, 0.125, 0.0)$ ,  $(2.5, 0.25, 0.0)$ ,  $(3.75, 0.375, 0.0)$  and  $(5.0, 0.0)$ , respectively. The results of relative errors and the number of Gaussian integral points are as shown in Table 4.

Table 2

The numerical results of singular integrals of quadrilateral elements ( $a=2$ )

Source points	Gaussian points	Proposed method	Gaussian points	Traditional method
$(0.0,0.0,0.0)$	200	6.13E-12	192	4.65E-11
$(0.25,0.125,0.0)$	576	1.52E-07	576	1.71E-04
$(0.5,0.25,0.0)$	576	2.57E-07	576	9.53E-05
$(0.75,0.375,0.0)$	576	3.57E-07	576	9.72E-06
$(1.0,0.5,0.0)$	384	7.92E-07	400	1.37E-05

Table 3

The numerical results of singular integrals of quadrilateral elements ( $a=5$ )

Source points	Gaussian points	Proposed method	Gaussian points	Traditional method
$(0.0,0.0,0.0)$	192	4.46E-12	200	3.02E-07
$(0.625,0.125,0.0)$	576	1.06E-07	576	7.41E-03
$(1.25,0.25,0.0)$	576	1.84E-07	576	5.97E-03
$(1.875,0.375,0.0)$	576	2.59E-07	576	3.31E-03
$(2.5,0.5,0.0)$	384	1.87E-07	400	5.54E-03

Table 4

The numerical results of singular integrals of quadrilateral elements ( $a=10$ )

Source points	Gaussian points	Proposed method	Gaussian points	Traditional method
$(0.0,0.0,0.0)$	192	3.69E-12	200	5.20E-06
$(1.25,0.125,0.0)$	576	8.51E-08	576	1.97E-02
$(2.5,0.25,0.0)$	576	1.50E-07	576	2.77E-02
$(3.75,0.375,0.0)$	576	2.13E-07	576	2.97E-02
$(5.0,0.5,0.0)$	384	4.77E-07	400	4.66E-02

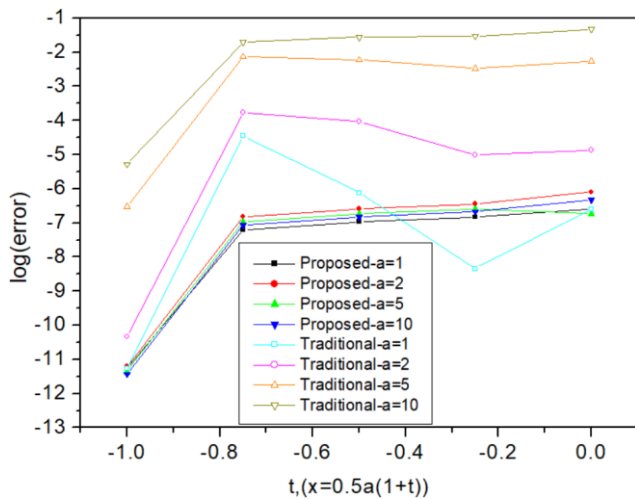


Fig. 9 The comparisons of relative errors with different source points

Fig. 9 shows the comparisons of relative errors with different source points and aspect ratios. From Table 1 – Table 4 and Fig. 6, it can be seen when using the same

Gaussian integral points, the accuracy of the proposed method has remained high with the increase of the aspect ratio of the integral element (even if the integral element becomes narrow and long). With the proposed method, the weakly singular integrals in the BIE can be accurately evaluated, at the same time, the influence of weak singular integrals can be eliminated in the solution of thin structural problems.

#### 4.2 The thin plate structure

In the second example, the proposed method is employed for the elastic analysis of thin plate structure. As shown in Fig. 10, the length, width and height of the thin plate are  $l=10$  mm and  $h=1$  mm. Young's modulus and Poisson's ratio are  $E=1$  MPa and  $\nu=0.25$ , respectively. To facilitate comparison, the quadratic displacement fields with an analytical solution are imposed on the boundary of the thin plate and the formulas are expressed as follows:

$$\begin{aligned} u_x &= -2x^2 + 3y^2 + 3z^2 \\ u_y &= 3x^2 - 2y^2 + 3z^2 \\ u_z &= 3x^2 + 3y^2 - 2z^2 \end{aligned} \quad (13)$$

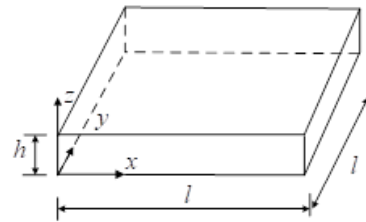


Fig. 10 The geometrical model of the thin plate

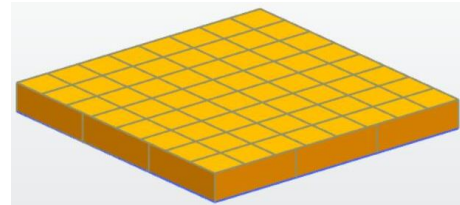


Fig. 11 The discrete model of the thin plate

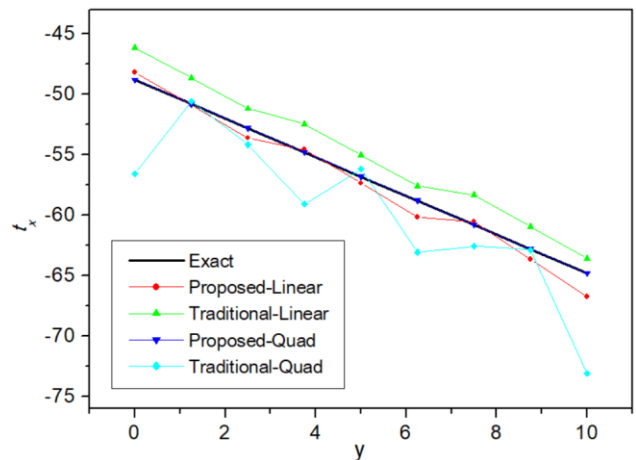


Fig. 12 The results of traction in the x direction

The geometrical model of the plate is discretized into 140 quadrilateral elements (Fig. 11). The flanks of the plate are discretized by several slender quadrilateral elements. A series of sample points are selected on line  $x=10$

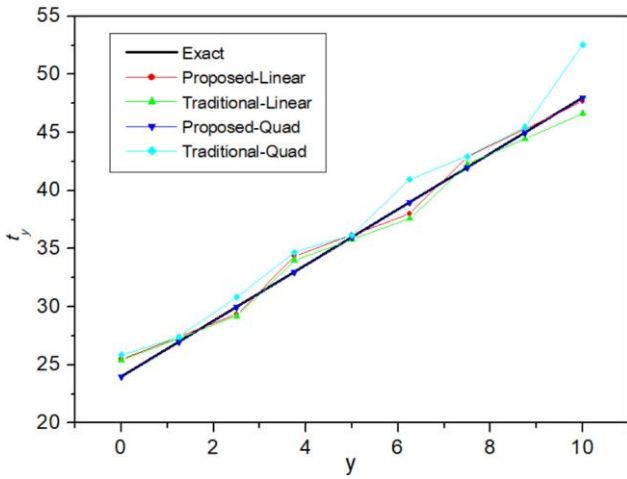


Fig. 13 The results of traction in the y direction

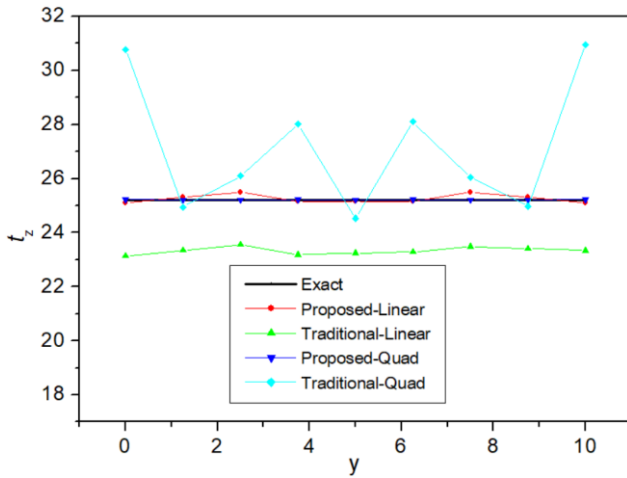


Fig. 14 The results of traction in the z direction

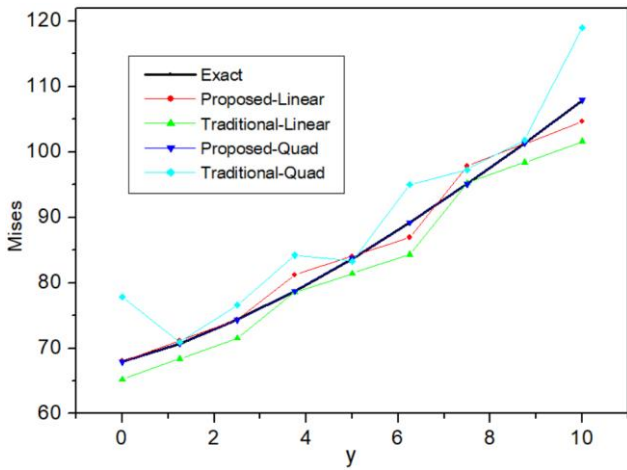


Fig. 15 The results of the Von Mises stress

and  $z=0.5$ . The numerical results obtained by applying the proposed method and the traditional method are as shown in Figs. 9 - 12. The symbols ‘proposed-Linear’, ‘proposed-Quad’, ‘Traditional-Linear’ and ‘Traditional-Quad’ denote the numerical results of the proposed method by using linear and quadratic elements, the numerical results of the traditional method by using linear and quadratic elements, respectively. It can be observed from Figs. 12 to 15, compared with the traditional method (coordinate transformation coupled with the traditional element subdivision method, in which the source point is directly connected with the element vertex), the numerical results of the proposed method are in better agreement with the analytical solution and have higher accuracy,

which further verify the accuracy and effectiveness of the proposed method.

### 4.3. The thin plate with a hole

To further verify the computational accuracy and generality of the proposed method, a thin plate with a hole is considered in the third example. The geometric parameters of the thin plate are as shown in Fig. 16. The Young’s modulus and Poisson’s ratio are  $E = 1 \text{ MPa}$ ,  $\nu = 0.25$ . Eq. (13) is treated as the boundary conditions which are imposed on the external boundary of the thin plate.

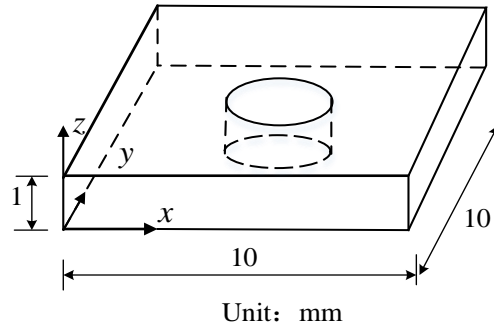


Fig. 16 The model of the plate with a hole

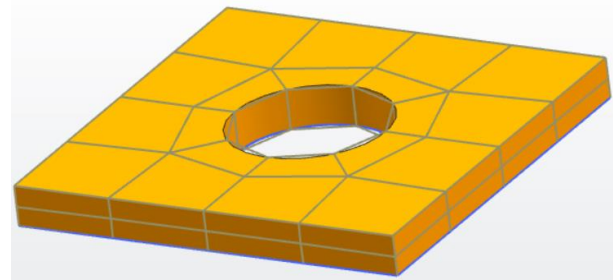


Fig. 17 The discrete model of the thin plate with a hole

80 quadrilateral elements with different shapes are used in all boundaries of the geometric model (Fig. 17 is the corresponding discrete model). The flanks of the model are discretized by several narrow elements. The sample points are selected on the centerline of the right side, and the numerical results obtained by using the proposed method and the traditional method are shown in Figs. 18 and 19.

It can be seen from Fig. 18 and Fig. 19, compared with the traditional method, the numerical results obtained

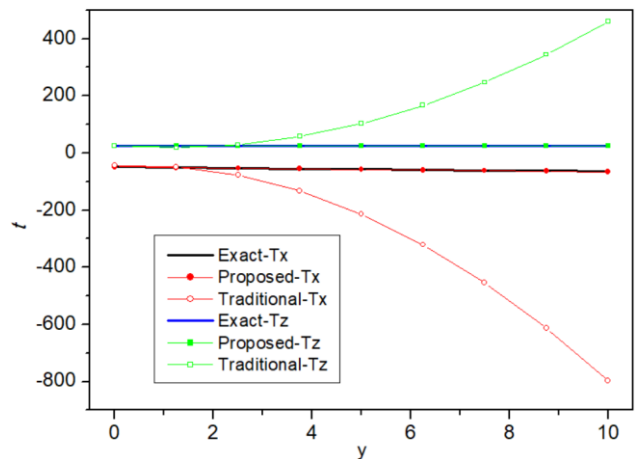


Fig. 18 The results of the traction in x and z direction

by the proposed method are in better agreement with the analytical solution and have higher computational accuracy, while the numerical results of the traditional method have diverged, which further verify the accuracy of the proposed method.

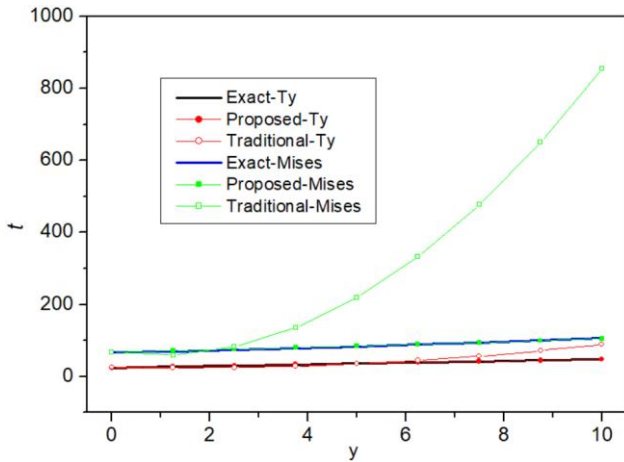


Fig. 19 The results of the Von Mises stress and the traction in y direction

4.4. The cylindrical revolution structures

To verify the validity and universality of the proposed method, a cylindrical revolution structure is considered in the last example. As shown in Fig.20, the geometric parameters of the model are:  $h=1.8$  m,  $r1=r3=1.8$  m,  $r4=2$  m,  $r2=2$  m. The material parameters are given as: Young's

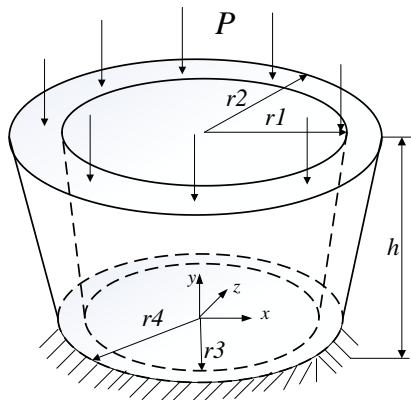


Fig. 20 The geometric model

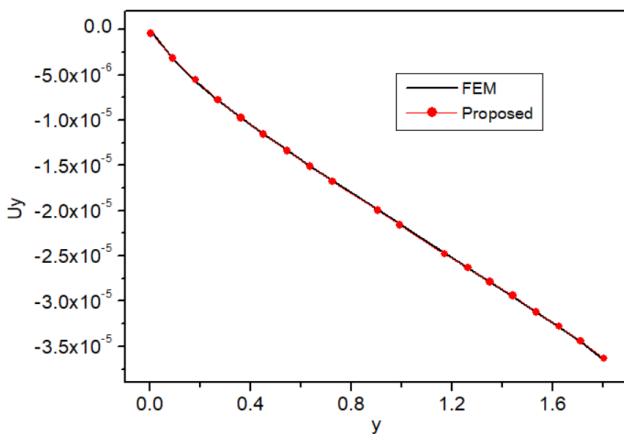


Fig. 21 The results of the displacement  $U_y$  on the line of external surface ( $z=0, x>0$ )

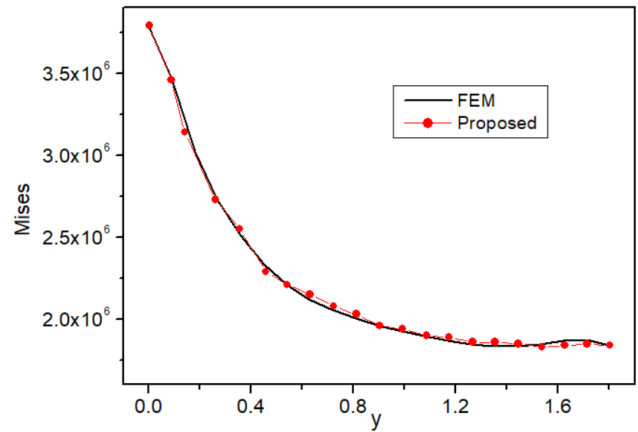


Fig. 22 The results of the Von Mises stress on the line of external surface ( $z=0, x>0$ )

modulus is 145 GPa, the density is 7800 kg/m<sup>3</sup>, and the Poisson's ratio is 0.25. The uniform press is 1 MPa. 96 quadratic elements are imposed in all the boundaries of the model. The results of FEM by using 54649 elements are regarded as a reference solution. The numerical results of the proposed method and FEM are as shown in Figs. 21 and 22.

It can be observed in Figs. 21 and 22, the numerical results obtained by the proposed method agree well with that obtained by the FEM, which further verify the validity of the proposed method.

5. Conclusions

Based on the properties of the weak singular integrals in the boundary integral equations of elastic problems, an element subdivision technique combined with  $\alpha\beta$  coordinate transformation method is proposed in this paper. The proposed method is simpler to implement, no matter where the source point is in the element, no matter what the element shape is, accurate and stable computational results can be obtained. Then, the proposed method is employed to analyze the thin-structural problem, and the numerical computational results show that the proposed method can be used to evaluate thin-structural problems accurately and efficiently.

Acknowledgments

This work was partly supported by key scientific and technological project of Henan Province (222102240077, 222102220106), and partly supported by Key Scientific Research Projects of Institutions of Higher Learning in Henan Province (21A460029 and 21A460030).

References

1. Sajedin, A.; Fard, M.; Khalkhali, A. 2019. Aero-structural study on the blade thickness effects in an automotive turbocharger turbine in transonic conditions, *Mechanika* 25(2): 134-140. <http://dx.doi.org/10.5755/j01.mech.25.2.22151>.
2. Jena, P.; Gupta, R. 2022. Estimation of delamination thickness in a multi-layered thermally thin structure by step heating thermography, *Composite Structures* 281: 114988. <http://dx.doi.org/10.1016/j.compstruct.2021.114988>.

3. **Zhang, Z.; Zhang, Y.; Liu, D.; Zhao, J.; Zhang, G.** 2022. Bubble behavior and its effect on surface integrity in laser-induced plasma micro-machining silicon wafer, *Journal of Manufacturing Science and Engineering* 144(9): 091008.  
<http://dx.doi.org/10.1115/1.4054416>.
4. **Xie, G.; Zhou, F.** 2020. A generation of special triangular boundary element shape functions for 3D crack problems, *Mathematical Problems in Engineering* 2020: 4629761.  
<http://dx.doi.org/10.1155/2020/4629761>.
5. **Cheng, A. H.; Cheng, D. T.** 2005. Heritage and early history of the boundary element method, *Engineering Analysis with Boundary Elements* 29: 268-302.  
<http://dx.doi.org/10.1016/j.enganabound.2004.12.001>.
6. **Liu, Y. J.** 2000. On the simple-solution method and non-singular nature of the BIE/BEM – a review and some new results, *Engineering Analysis with Boundary Elements* 24: 789-795.  
[http://dx.doi.org/10.1016/S0955-7997\(00\)00061-8](http://dx.doi.org/10.1016/S0955-7997(00)00061-8).
7. **Chen, J. T.; Kao, J. H.; Kao, S. K.; Lee, Y. T.; Kuo, S. R.** 2022. Study on the double-degeneracy mechanism of BEM/BIEM for a plane elasticity problem with line segments, *Engineering Analysis with Boundary Elements* 136: 290-302.  
<http://dx.doi.org/10.1016/j.enganabound.2021.12.002>.
8. **Feng, S. Z.; Han, X.** 2019. A novel multi-grid based re-analysis approach for efficient prediction of fatigue crack propagation, *Computer Methods in Applied Mechanics and Engineering* 353: 107-122.  
<http://dx.doi.org/10.1016/j.cma.2019.05.001>.
9. **Wang, Q.; Feng, Y. T.; Zhou, W.; Cheng, Y.; Ma, G.** 2020. A phase-field model for mixed-mode fracture based on a unified tensile fracture criterion, *Computer Methods in Applied Mechanics and Engineering* 370(15): 113270.  
<http://dx.doi.org/10.1016/j.cma.2020.113270>.
10. **Liu, X.; Wu, H.; Sun, R.; Jiang, W.** 2022. A fast multipole boundary element method for half-space acoustic problems in a subsonic uniform flow, *Engineering Analysis with Boundary Elements* 137: 16-28.  
<http://dx.doi.org/10.1016/j.enganabound.2022.01.008>.
11. **Lu, C.; Chen, L.; Chen, H.** 2021. Shape optimization of acoustic barriers based on subdivision surfaces BEM, *International Journal of Computational Methods and Experimental Measurements* 9(2): 108-116.  
<http://dx.doi.org/10.2495/CMEM-V9-N2-108-116>.
12. **Yao, Z.; Zheng, X.; Yuan, H.; Jin, F.** 2019. Research progress of high-performance BEM and investigation on convergence of GMRES in local stress analysis of slender real thin-plate beams, *Engineering Computations* 36: 2530-2556.  
<http://dx.doi.org/10.1108/EC-10-2018-0477>.
13. **Gu, Y.; Lei, J.** 2021. Fracture mechanics analysis of two-dimensional cracked thin structures (from micro-to nano-scales) by an efficient boundary element analysis, *Results in Applied Mathematics* 11: 100172.  
<https://doi.org/10.1016/j.rinam.2021.100172>.
14. **Jaskowicz, J.; Stankiewicz, A.; Pluciński, P.** 2020. Three-dimensional numerical modelling of multi-layered shell structures using two-dimensional plane mesh, *Advances in Engineering Software* 149: 102840.  
<http://dx.doi.org/10.1016/j.advengsoft.2020.102840>.
15. **Zhou, H.; Niu, Z.; Cheng, C.; Guan, Z.** 2008. Analytical integral algorithm applied to boundary layer effect and thin body effect in BEM for anisotropic potential problems, *Computers & Structures* 86: 1656-1671.  
<http://dx.doi.org/10.1016/j.compstruc.2007.10.002>.
16. **Niu, Z. R.; Wendland, W. L.; Wang, X.; Zhou H.** 2005. A semi-analytical algorithm for the evaluation of the nearly singular integrals in three-dimensional boundary element methods, *Computer Methods in Applied Mechanics and Engineering* 194(9-11): 1057-1074.  
<http://dx.doi.org/10.1016/j.cma.2004.06.024>.
17. **Zhong, Y.; Xie, G.; Hou, J.; He, W.; Wang, S.** 2021. A boundary weak singularity elimination method for multilayer structures, *Engineering Analysis with Boundary Elements* 130: 69-78.  
<http://dx.doi.org/10.1016/j.enganabound.2021.05.012>.
18. **Xie, G.; Zhou, F.; Zhong, Y.; Geng, H.; Wu, C.** 2020. Bi-directional sinh transformations based on the generalized Duffy space for nearly singular integrals, *Journal of Computational and Applied Mathematics* 380: 112981.  
<http://doi.org/10.1016/j.cam.2020.112981>.
19. **Zhang, Y.; Li, X.; Sladek, V.; Sladek, J.; Gao, X.** 2015. A new method for numerical evaluation of nearly singular integrals over high-order geometry elements in 3D BEM, *Journal of Computational and Applied Mathematics* 277: 57-72.  
<https://doi.org/10.1016/j.cam.2014.08.027>.
20. **Zhong, Y.; Hou, J.; Feng, S.; Xie, G.; Wang, X.; He, W.; Wang, L.; Chen, Z.; Hao, H.** 2021. BEM analysis of multilayer thin structures using a composite transformation method for boundary integrals, *Engineering Analysis with Boundary Elements* 134: 650-664.  
<http://dx.doi.org/10.1016/j.enganabound.2021.11.007>.
21. **Chen, J.; Kao, J.; Kao, S.; Lee, Y.; Kuo, S.** 2022. Study on the double-degeneracy mechanism of BEM/BIEM for a plane elasticity problem with line segments, *Engineering Analysis with Boundary Elements* 136: 290-302.  
<http://dx.doi.org/10.1016/j.enganabound.2021.12.002>.
22. **Tsamasphyros, G. J.; Theotokoglou, E. E.; Filopoulos, S. P.** 2013. Study and solution of BEM-singular integral equation method in the case of concentrated loads, *International Journal of Solids & Structures* 50: 1634-1645.  
<http://dx.doi.org/10.1016/j.ijsolstr.2013.01.032>.
23. **Sladek, J.; Sladek, V.; Krivacek, J.; Aliabadi M.** 2007. Local boundary integral equations for orthotropic shallow shells, *International Journal of Solids & Structures* 44: 2285-2303.  
<http://dx.doi.org/10.1016/j.ijsolstr.2006.07.010>.
24. **Klees, R.** 1996. Numerical calculation of weakly singular surface integrals, *Journal of Geodesy* 70: 781-797.  
<http://dx.doi.org/10.1007/BF00867156>.
25. **Gao, X.; Zhang, J.; Zheng, B.; Zhang, C.** 2016. Element-subdivision method for evaluation of singular integrals over narrow strip boundary elements of super thin and slender structures, *Engineering Analysis with Boundary Elements* 66: 145-154.  
<http://dx.doi.org/10.1016/j.enganabound.2016.02.002>.
26. **Zhang, J.; Chi, B.; Singh, K.; Zhong, Y.; Ju, C.** 2019. A binary-tree element subdivision method for evaluation of nearly singular domain integrals with continuous or

- discontinuous kernel, *Journal of Computational and Applied Mathematics* 362: 22-40.  
<http://dx.doi.org/10.1016/j.cam.2019.04.027>.
27. **Telles, J.** 1987. A self-adaptive co-ordinate transformation for efficient numerical evaluation of general boundary element integrals, *International Journal for Numerical Methods in Engineering* 24: 959-973.  
<http://dx.doi.org/10.1002/nme.1620240509>.
28. **Johnston, P. R.; Elliott, D.** 2001. A generalisation of Telles' method for evaluating weakly singular boundary element integrals, *Journal of Computational and Applied Mathematics* 131: 223-243.  
[http://dx.doi.org/10.1016/s0377-0427\(00\)00273-9](http://dx.doi.org/10.1016/s0377-0427(00)00273-9).
29. **Xie, G.; Zhong, Y.; Zhou, F.** et al. 2020. Singularity cancellation method for time-domain boundary element formulation of elastodynamics: a direct approach, *Applied Mathematical Modelling* 80: 647-667.  
<http://dx.doi.org/10.1016/j.apm.2019.11.053>.
30. **Zhu, M. D.; Sarkar, T. K.; Zhang, Y.** 2021. On the shape-dependent problem of singularity cancellation transformations for weakly near-singular integrals, *IEEE Transactions on Antennas and Propagation* 69: 5837-5850.  
<http://dx.doi.org/10.1109/TAP.2021.3069483>.
31. **Rong, J. J.; Wen, L. H.; Xiao, J. Y.** 2014. Efficiency improvement of the polar coordinate transformation for evaluating BEM singular integrals on curved elements, *Engineering Analysis with Boundary Elements* 38: 83-93.  
<http://dx.doi.org/10.1016/j.enganabound.2013.10.014>.
32. **Johnston, P. R.** 1999. Application of sigmoidal transformations to weakly singular and near-singular boundary element integrals, *International Journal for Numerical Methods in Engineering* 45: 1333-1348.  
[https://doi.org/10.1002/\(SICI\)10970207\(19990810\)45:10<1333:AID-NME632>3.0.CO;2-Q](https://doi.org/10.1002/(SICI)10970207(19990810)45:10<1333:AID-NME632>3.0.CO;2-Q).
33. **Gao, X. W.** 2022. A boundary element method without internal cells for two-dimensional and three-dimensional elastoplastic problems, *Journal of Applied Mechanics* 69: 154-160.  
<http://dx.doi.org/10.1115/1.1433478>.
34. **Brebbia, C. A.** 1981. *Boundary Element Methods*; Springer-Verlag: Berlin, Germany, ISBN:3540108165.
35. **Sladek, V.; Sladek, J.; Tanaka, M.** 1993. Regularization of hypersingular and nearly singular integrals in the potential theory and elasticity, *International Journal for Numerical methods in Engineering* 36: 1609-1628.  
<http://dx.doi.org/10.1002/nme.1620361002>.
36. **Guiggiani, M.; Gigante, N.** 1990. A general algorithm for multi-dimensional Cauchy principal value integrals in the boundary element method, *ASME Journal of applied Mechanics* 57: 906-915.  
<http://dx.doi.org/10.1115/1.2897660>.
37. **Zhang, J.; Qin, X.; Han, X.; Li G.** 2009. A boundary face method for potential problems in three dimensions, *International Journal for Numerical Methods in Engineering* 80: 320-337.  
<http://dx.doi.org/10.1002/nme.2633>.

J. Hou, L. Zeng, Y. Zhong, D. Zhao, M. Zhao

#### A SUBDIVISION TRANSFORMATION METHOD FOR WEAKLY SINGULAR BOUNDARY INTEGRALS IN THIN-STRUCTURAL PROBLEM

#### S u m m a r y

A subdivision transformation method evaluated for weakly singular integrals is proposed in this paper, and the method is implemented as follows: based on the position of the source points, the shape information of the elements and the nearest distance from the source point to the integral element, a subdivision technology is constructed at first. With this subdivision technology, the integral element can be divided into several integral blocks with good shapes. And then, a simpler coordinate transformation method is constructed to remove the weak singularities of the integral blocks obtained by the subdivision technology. Compared with the conventional polar coordinate transformation method, the present transformation method does not need to calculate their integral interval, which is simpler and more effective to implement. Finally, the paper gives three numerical examples to verify the accuracy and validity of the present method.

**Keywords:** elasticity problem, boundary integral equation, singular integrals, element subdivision, coordinate transformation.

Received June 26, 2022

Accepted June 14, 2023



This article is an Open Access article distributed under the terms and conditions of the Creative Commons Attribution 4.0 (CC BY 4.0) License (<http://creativecommons.org/licenses/by/4.0/>).